Time-Resolved Infrared Reflectance Studies of the Dehydration-Induced Transformation of Uranyl Nitrate Hexahydrate to the Trihydrate Form

Timothy J. Johnson,[1] Lucas E. Sweet,[1] David E. Meier,[1] Edward J. Mausolf,[1,2] Eunja Kim,[3] Philippe F. Weck,[4] Edgar C. Buck[1], Bruce K. McNamara[1]*

[1]Pacific Northwest National Laboratory, 902 Battelle Blvd. P.O. Box 999, Mail Stop K3-61, Richland, Washington 99352, United States

[2]Department of Chemistry and Harry Reid Center for Environmental Studies, University of Nevada Las Vegas, 4505 Maryland Parkway, Las Vegas, Nevada 89154, United States

[3]Department of Physics and Astronomy, University of Nevada Las Vegas, 4505 Maryland Parkway, Las Vegas, Nevada 89154, United States

[4]Sandia National Laboratories, P.O. Box 5800, MS 0779, Albuquerque, New Mexico 87185, United States

KEYWORDS. Uranyl nitrate, uranyl nitrate hexahydrate, uranyl nitrate trihydrate, infrared spectroscopy, reflectance spectroscopy, reststrahlen bands, microscopy, x-ray diffraction, density functional theory.

ABSTRACT: Uranyl nitrate is a key species in the nuclear fuel cycle. However, this species is known to exist in different states of hydration, including the hexahydrate ($[UO_2(NO_3)_2(H_2O)_6]$ often called UNH), the trihydrate $[UO_2(NO_3)_2(H_2O)_3$ or UNT], and in very dry environments the dihydrate form $[UO_2(NO_3)_2(H_2O)_2]$. Their relative stabilities depend on both water vapor pressure and temperature. In the 1950s and 1960s the different phases were studied by infrared transmission spectroscopy, but were limited both by instrumental resolution and by the ability to prepare the samples for transmission. We have revisited this problem using time-resolved reflectance spectroscopy, which requires no sample preparation and allows dynamic analysis while the sample is exposed to a flow of N_2 gas. Samples of known hydration state were prepared and confirmed via X-ray diffraction patterns of known species. In reflectance mode the hexahydrate $UO_2(NO_3)_2(H_2O)_6$ has a distinct uranyl asymmetric stretch band at 949.0 cm^{-1} that shifts to shorter wavelengths and broadens as the sample desiccates and recrystallizes to the trihydrate, first as a shoulder growing in on the blue edge but ultimately results in a doublet band with reflectance peaks at 966 and 957 cm^{-1}. The data are consistent with transformation from UNH to UNT as UNT has two inequivalent UO_2^{2+} sites. The dehydration of $UO_2(NO_3)_2(H_2O)_6$ to $UO_2(NO_3)_2(H_2O)_3$ is both a structural and morphological change that has the lustrous lime green $UO_2(NO_3)_2(H_2O)_6$ crystals changing to the matte greenish yellow of the trihydrate solid. The phase transformation and crystal structures were confirmed by density functional theory calculations and optical microscopy methods, both of which showed a transformation with two distinct sites for the uranyl cation in the trihydrate, while one in the hexahydrate.

1. INTRODUCTION

Uranyl nitrate hexahydrate [$UO_2(NO_3)_2(H_2O)_6$], often termed UNH, is a key intermediate in the uranium fuel cycle both for ore processing and spent fuel re-processing. The dehydration of UNH is an involved process that can pass through various intermediate phases, including uranyl nitrate trihydrate (UNT) and uranyl nitrate dihydrate (UND). The stability of uranyl nitrate and its sundry hydration state species have been studied for several decades.[1-7] Bordère et al.[1] demonstrated that dehydration is only complete prior to de-nitration, if the residual pressure above the specimen is < 20 mbar. They recognized two transformation conditions: At higher pressures, an instantaneous nucleation and 2-dimensional nuclei growth occur; conversely, lowering the pressure favors a 2-dimensional interfacial advancement mechanism. It was found that the residual pressure dictated the growth or dehydration mechanism and explained the abnormal variation in dehydration rates, a phenomenon termed the Smith-Topley effect.[6]

However, while infrared transmission of UNH was studied long ago,[8-11] the dehydration processes of this material have never been studied by reflectance spectroscopy, nor *ab initio* quantum mechanical methods. By determining the hydration - desiccation state of the uranyl nitrate phases, and monitoring these changes with reflectance infrared spectroscopy, it may be possible to understand these phases' chemical states and processing history. Earlier work on the phases of uranyl nitrates typically used transmission infrared spectroscopy with specimens mixed as Nujol mulls or pressed into IR-transparent KBr pellets.[8-11] The early studies were limited in their ability to distinguish the nature of these uranyl phases, due in part to lower spectral resolution of the day and in part due to the requisite sample manipulation needed for transmission measurements. As a result, we have revisited these studies to assess the change in phases with relative humidity for the IR spectra and the thresholds for such conditions. Previous studies[1-11] have shed light on the kinetics of uranyl nitrate system; the objective of the present paper is to use time-resolved IR reflectance spectroscopy for distinguishing these changes with relative humidity, the thresholds to such changes and the potential for establishing the history of environmental uranyl nitrate samples.

Uranyl Nitrate Structures. The uranyl nitrate hydrate phases are based upon isolated clusters of [$(UO_2)(H_2O)_2(NO_3)_2$] each containing a linear uranyl ion (UO_2^{2+}) with local $D_{\infty h}$symmetry.[10,11] The structures of $UO_2(NO_3)_2(H_2O)_6$,[12] $UO_2(NO_3)_2(H_2O)_3$,[13] as well as the

dihydrate $UO_2(NO_3)_2(H_2O)_2$,[14] have all been described. These compounds crystallize in the space groups $Cmc2_1$, $P\bar{1}$, and $P2_1/c$, respectively. In UNT, there are two symmetrically distinct U^{VI} atoms, hereafter referred to as U_1 (on 1*h* Wyckoff sites; $\bar{1}$ symmetry) and U_2 (on 1*d* Wyckoff sites; $\bar{1}$ symmetry), both of which are part of linear $(UO_2)^{2+}$ uranyl ions and which are coordinated by six equatorial O atoms forming hexagonal bipyramids. This is juxtaposed to UNH, however, [12] where there is a single unique position for the U^{VI} atom (on 4*a* Wyckoff sites, *m* symmetry) and associated uranyl ion as described below.

Infrared spectroscopy is particularly well suited to study such phenomena since the method can observe subtle frequency shifts that arise due to local environmental or neighboring chemical effects, thus leading to high specificity for chemical assignments. Infrared spectroscopy on (organic) solids has traditionally been performed by mixing dilute solutions of the analyte in an alkali halide (e.g. KBr) which is pressed into a transparent pellet or, alternatively, grinding and placing the sample as a Nujol or fluorolube mull atop an IR-transparent substrate such as ZnSe. In the case of organic and inorganic salts, however, pressing the alkali halide pellet can lead to either ion metathesis[16] or, as in the present case of UNH, potential dehydration reactions.[5,9,10] Such IR sampling methods are not only slow and invasive, but also preclude any (heterogeneous) kinetic studies of the solids of interest interacting with gases in their local environment. We have therefore chosen to use solid reflectance spectroscopy on the bulk material. It is aptly suited for such studies as the bulk material can be monitored in real time as it is continuously exposed to both the incoming IR radiation and (if desired) a flow of gas, which was the method used for the present investigations.

2. EXPERIMENTAL SECTION

Infrared Spectroscopy. For the time-resolved reflectance IR studies we employed our recently developed system that records the directional-hemispherical infrared reflectance spectra of solid samples so as to capture both the diffuse and specular light components that are scattered into the 2π steradians of a hemisphere.[17-19] The method places a few grams of solid powder into an open 1.9-cm diameter sample cup at the bottom of an integrating sphere. Spectra are ratioed relative to a spectrum that also has sample in the cup (for constant sphere albedo) but has the IR beam pointed at another point on the sphere wall. Results are then reported as %R reflectance. The

Bruker A562 sphere used here also contains a gas inlet port to purge the sphere, in this case with nitrogen gas of very low and controlled humidity. The A562 was permanently bolted to a Bruker Matrix/M IRCube infrared spectrometer equipped with a glow bar source, a KBr beamsplitter and an external detector electronic input for the mid-band MCT detector (2 x 2 mm element) which is attached to the A562. Spectra were recorded in time-resolved fashion at 1.0 minute intervals using Bruker's OPUS 6.5 software; for each spectrum 200 interferograms were averaged before the next 1 minute interval acquisition was initiated. Interferograms were recorded at 4.0 cm^{-1} resolution and Fourier-transformed using the Mertz phase correction and a Blackman-Harris 3-term apodization function.

Optical Microscopy. Optical microscopy was performed using a Nikon 400POL Polarizing Light microscope equipped with an ARC-2 Paxcam digital camera. Images were obtained automatically over various stages of desiccation. Length scale was calibrated with a National Institute of Standards and Technology (NIST)-2800 microscopy standard.

X-ray Diffraction. Each uranyl nitrate sample was analyzed using a Rigaku/Ultima IV X-ray Diffraction (XRD) unit equipped with a silicon linear position sensitive detector and graphite monochromated copper X-ray tube (Kα radiation, λ = 1.5406 Å). Diffraction data were collected from 5° to 90° 2θ with a step size of 0.02 and a scan speed of 3° per minute. Phase identification was performed using EVA (Bruker) search match software linked to the 2013 Powder Data File 4 (ICDD). Full pattern Rietveld refinements used extract the relative weight percentages of the different uranyl nitrate phases present in each sample were conducted using the TOPAS (Bruker) software package. A hermetically sealed sample holder was used to maintain the hydration state of the uranyl nitrate phase formed while diffraction data were collected.

Computational Methods. First-principles total energy calculations were performed using the spin-polarized density functional theory (DFT), as implemented in the Vienna *ab initio* simulation package (VASP). The exchange-correlation energy was calculated using the generalized gradient approximation (GGA), with the parameterization of Perdew and Wang (PW91).[21] The PW91 functional was found in previous studies to correctly describe the geometric parameters and properties of various uranium-containing structures.[22,23] Although theoretical approaches that go beyond standard DFT are needed to account for the strong on-site Coulomb repulsion between U 5*f* electrons in bulk UO_2, previous studies on uranyl peroxide

phases and uranyl-organic coordination compounds by Weck et al. showed that[22,23] standard DFT is appropriate to describe the uranyl nitrate systems in this study.

The interaction between valence electrons and ionic cores was described by the projector augmented wave (PAW) method. The U(6*s*,6*p*,6*d*,5*f*,7*s*), O(2*s*,2*p*) and N(2*s*,2*p*) electrons were treated explicitly as valence electrons in the Kohn-Sham (KS) equations and the remaining core electrons together with the nuclei were represented by PAW pseudo-potentials. The KS equations were solved using the blocked Davidson iterative matrix diagonalization scheme followed by the residual vector minimization method. The plane-wave cutoff energy for the electronic wavefunctions was set to a value of 500 eV, ensuring the total energy of the system to be converged to within 1 meV per atom. Electronic relaxation was performed with the residual minimization method direct inversion in the iterative subspace (RMM-DIIS), preconditioned with residuum-minimization. Ionic relaxation was carried out using the conjugate-gradient algorithm and the Hellmann-Feynman forces acting on atoms were calculated with a convergence tolerance set to 0.01 eV/Å. A periodic unit cell approach was used in the calculations and structural relaxation was performed without symmetry constraints. The Brillouin zone was sampled using the Monkhorst-Pack *k*-point scheme with a *k*-point mesh of 3×3×3. The structures of $UO_2(NO_3)_2(H_2O)_6$,[12] $UO_2(NO_3)_2(H_2O)_3$,[13] and $UO_2(NO_3)_2(H_2O)_2$ [14] characterized experimentally were used as initial guesses in structural relaxation calculations. Using the structures relaxed with DFT, density functional perturbation theory (DFPT) linear response calculations were carried out at the GGA/PW91 level of theory with VASP to determine the vibrational frequencies and associated intensities. The latter were computed based on the Born effective charges (BEC) tensor, which corresponds to the change in atoms polarizabilities with respect to an external electric field. No symmetry constraints were applied in DFPT calculations.

3. RESULTS

Optical Microscopy. To investigate the growth kinetics of UNT from a UNH parent sample, we first conducted *in situ* optical microscopy measurements. Figure 1 shows *in situ* polarized light microscopy images. As the UNH was allowed to precipitate from the uranyl nitrate liquor, it gradually started to dehydrate. The rate of the dehydration was dependent on the RH as also

observed in the IR experiments below. The recrystallization was pseudomorphic, in other words, the trihydrate formed within the existing hexahydrate crystals. The crystallite size was far smaller than the original $UO_2(NO_3)_2(H_2O)_6$. This morphological transformation likely accounts for the dull appearance of the UNT relative to the luster of the $UO_2(NO_3)_2(H_2O)_6$ crystals as seen in Figure 2. The smaller particle size will also influence the XRD signal and the IR signal compared to the signal generated by the freshly formed $UO_2(NO_3)_2(H_2O)_3$.

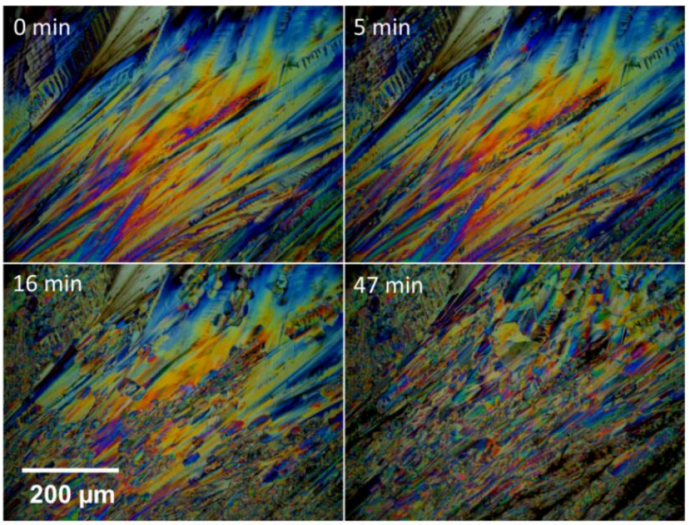

Figure 1. Optical micrographs showing the pseudomorphic crystallization of uranyl nitrate trihydrate following the dehydration of uranyl nitrate hexahydrate due to flow of dry nitrogen gas.

Additional images showing the recrystallization phenomena are provided in the Supplementary section (Figure S2, S3, and S4). The time shown in each panel represents the elapsed time from the initial measurement. The interface clearly moves randomly accompanying the phase transformation from UNH to UNT with the elapse of time. [Real time precipitation of $UO_2(NO_3)_2(H_2O)_6$ and transformation to UNT is shown in the Supporting Information, Movie 1].

Consistent with the IR and XRD results at low humidity (< ca. 10%) the phase transformation appears nearly complete in less than an hour or so. During this process, the movie shows the simultaneous occurrence of dissolved uranyl nitrate, precipitating $UO_2(NO_3)_2(H_2O)_6$, and UNT forming behind the precipitating front. The movie unambiguously shows that the phase transformation occurs through the recrystallization of a new phase. Thermally excited atoms will rearrange to their lowest energy sites to form UNT structure at the expense of $UO_2(NO_3)_2(H_2O)_6$.

Since the time scale for the crystal growth is related to the speed of atomic rearrangement, it takes shorter time at higher temperature and vice-versa.

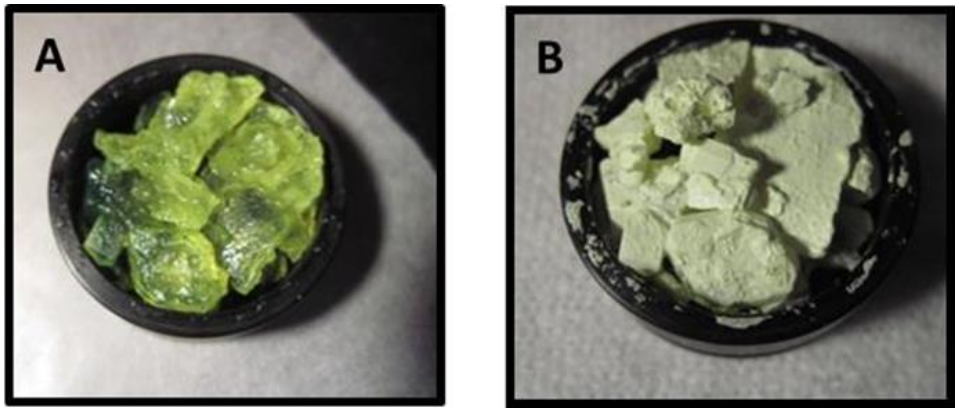

Figure 2 Photographs of uranyl nitrate samples for IR experiments determined by XRD to be (**A**) $UO_2(NO_3)_2(H_2O)_6$ and (**B**) a mixture of 16% $UO_2(NO_3)_2(H_2O)_6$ and 84% $UO_2(NO_3)_2(H_2O)_3$ (see Fig. 5).

Infrared Reflectance Spectroscopy Desiccation Experiments. Whereas the above experiments showed that at low humidity the UNH to UNT desiccation (presumably even to UND) can occur on the timescale of ~1 hour, it was also desired to observe the spectral changes when such desiccation phase changes take place. It was further desired to associate chemical identities with the species observed in the dehydration (and presumably rehydration) experiments. To that end XRD measurements and time-resolved infrared reflectance experiments were conducted using dried nitrogen gas so as to effect such spectral changes: the IR kinetic results are shown in Figures 3 and 4. For these experiments the parent starting material was confirmed by XRD to be 100% uranyl nitrate hexahydrate (see Figure 2 and 5). The flow rate for the experiment was 0.5 SLM of $CaSO_4$-dried house N_2 gas originating from a liquid nitrogen Dewar boil-off. The spectra were recorded at 1.0 min intervals but Figures 3 and 4 plot only every 10^{th} spectrum for clarity; there is one gap (approx. 11 minutes) where software collection stopped and had to be re-initiated; the displayed spectra are centered about the start and end of that gap. We also note that the first spectrum does not strictly correspond to time t = 0 as the sample had to be loaded into the sample cup, placed in the A562 sphere and the reference spectrum recorded; these activities were estimated to be of approximately 5 minutes duration.

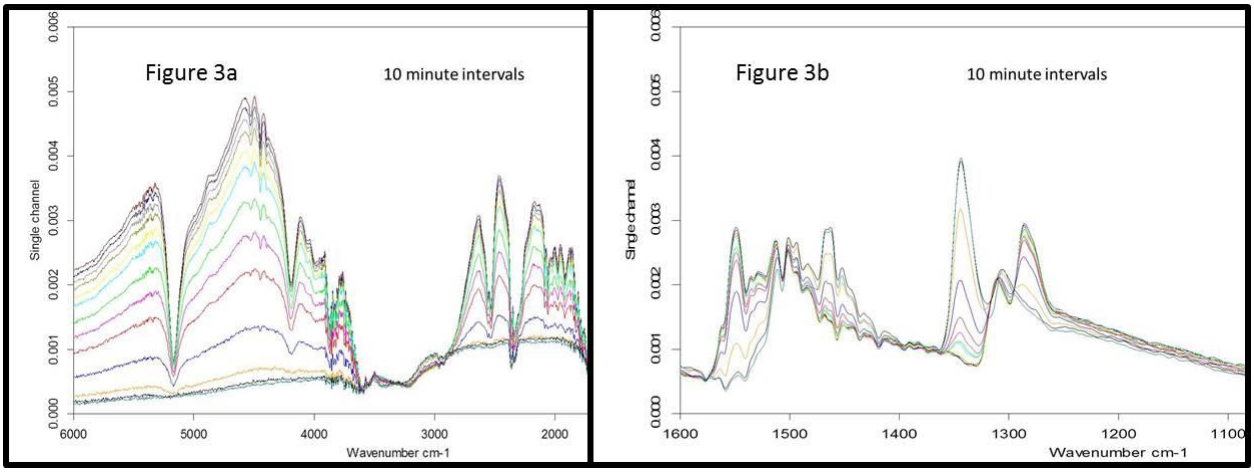

Figure 3. Time dependent (Δt = 10 min) IR reflectance spectra showing the overall reflectivity increase for a) 6000 – 1600 cm^{-1} region and b) the longwave 1600 to 1100 cm^{-1} region with some features increasing in intensity, others decreasing.

Reflectance spectra are more complicated to interpret than IR transmission spectra: As pointed out by Bertie[24] and others[20,25-28] it is incorrect to directly compare the positions of absorption and reflectance peak positions as reflectance bands involve both the real as well as the imaginary component of the refractive index, whereas for absorption bands it is only the imaginary component that gives rise to the signal. In general, in the visible and shortwave infrared surface scattering tends to dominate reflectance spectra of Lambertian samples which show high %R values for small particles as long as there are few or no absorption bands present. When there are weak to medium absorption bands (i.e. with small but non-zero k values) they manifest themselves as downward-going peaks due to light extinction (Fig. 3a). In the longwave infrared, however, there are often exceptions to this due to certain phenomena known as reststrahlen bands: These are characterized by large values for both optical constants n and k, and typically result in surface scattering of the light which manifests itself as upward-going peaks.[20,25-28] For many different types of powders where volume scattering dominates, such reflectance spectra tend to be strongly particle-size dependent; smaller particle sizes result in higher albedo, i.e. higher overall reflectivity. For reststrahlen-type features, however, the reflection band amplitudes tend to be relatively invariant to the average particle size in the LWIR.[20,26] The spectra seen in Figure 3b and Fig. 4 exhibit such bands as the UNH sample is being desiccated by the dry N_2 purge over a course of 2.7 hours. In the shorter wavelength region between 6,000 and 1,600 cm^{-1} the overall reflectivity simply increases as a function of time. This is ascribed to the relatively pure UNH crystals desiccating; the sample undergoes a morphological change

which was seen under the polarized light of the microscope as recrystallization. To the naked eye, the materials transform from translucent lime-green crystals to a matte greenish yellow powder. At the same time in the visible and near-IR spectra we observe, for the same physical transformation, more diffuse spectral scattering. The increased Lambertian scattering is seen both in the spectra of Figure 3a and the photo of Figure 2.

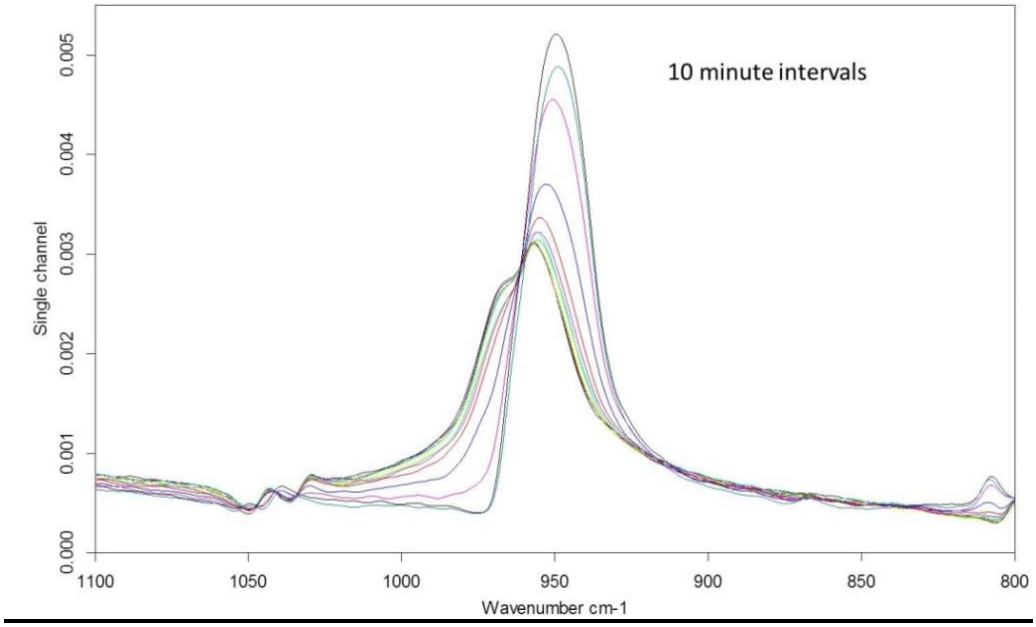

Figure 4. IR reflectance spectra of UNH to UNT transformation accompanied by emergence of doublet peaks at 957 and 966 cm^{-1} that may be ascribed to the UO_2^{2+} asymmetric stretch in the trihydrate moiety.

As seen in Figure 3b and 4, however, the results for the longwave infrared (LWIR) are more complicated: Certain new upward-going bands grow in such as the peaks at 1286 and 1549 cm^{-1} while other peaks disappear such as the bands at 1344 and 1462 cm^{-1}. We ascribe the 1344 band disappearance and the 1286 cm^{-1} band evolution with the removal of the water and realignment of the ions, especially the NO_3^- ions, within the unit cell as discussed below.

A portion of the chemical transformation spectrum is also displayed in Figure 4 for the very strong reststrahlen feature shifting (first as a shoulder) to higher frequencies and ultimately resulting in a doublet band with peaks at 957 and 966 cm^{-1}. We ascribe the original upward-going peak (seen at 949.0 cm^{-1} in the earliest spectra) to the reststrahlen band associated with the ν_3 band of the asymmetric uranyl stretch of the parent hexahydrate.[30] These are some of the same UO_2^{2+} IR bands that were seen in absorption mode for UNH by Gatehouse and Comyns[7] and

Allpress and Hambly[8] as well as for several analogous uranyl complexes as studied later by other workers.[9-11,33,34] This band is typical of a reststrahlen band in that it displays quite a large reflectivity often seen for bands with strong absorption features.[20,25-29,35-37] For the earliest time slices in Figure 4, adjacent to the 949 band is a minimum at 973 cm^{-1}, seen as a sharp drop in reflectivity occurring on the high frequency side of the ν_3 reststrahlen band. Such features are often seen in the reflectance spectra of powdered minerals and are termed a Christiansen minimum,[20,35-37] always appearing on the short wavelength edge of the reststrahlen band. The minima are ascribed to the region where the refractive index undergoes a rapid change such that the refractive index approaches the refractive index of the surrounding medium (i.e. n=1 for air) resulting in no scattering or absorption, i.e. a zero minimum in reflectance.[20,25,35-37]

At the conclusion of the infrared experiment the sample was transported to another laboratory where XRD analysis showed the desiccated sample to be 84% UNT and 16% remaining of the original UNH (Figures 2 and 5). For the resultant spectra in Figure 4 we ascribe the pair of doublet peaks seen at 957 and 966 cm^{-1} to the UO_2^{2+} asymmetric stretch[8-11] of the resultant UNT moiety.[10,13]This is the same asymmetric stretch mode of the UO_2^{2+} cation of the UNH starting material, but in the UNT product there are two non-equivalent sites[13]for the uranyl cation in each triclinic unit cell. We propose that the two non-equivalent position result in two distinct frequencies (957 and 966 cm^{-1}) for the asymmetric O-U-O stretching frequency; the same is presumably true for the symmetric mode which would be seen via Raman spectroscopy.[10,11,38]

X-ray diffraction. The x-ray diffraction data indicated that the sample of uranyl nitrate that was provided for the time resolved IR experiment was initially pure UNH. After being exposed to the dry nitrogen flow for ~2.7 hours, the sample was seen as a slightly green but mostly matte yellow-green powder (Fig. 2) and analyzed by XRD methods. Full pattern Rietveld refinement was performed on the x-ray diffraction data. The data collected immediately after the IR measurements indicated that 84% of the sample had converted to $UO_2(NO_3)_2(H_2O)_3$ while the remaining 16% was still $UO_2(NO_3)_2(H_2O)_6$. The fits are shown in the bottom trace of Figure 5 with the pattern of $UO_2(NO_3)_2(H_2O)_6$ in blue, and the $UO_2(NO_3)_2(H_2O)_3$ pattern in red. Peak intensities are scaled to match those of the pattern obtained after the IR dehydration experiment.

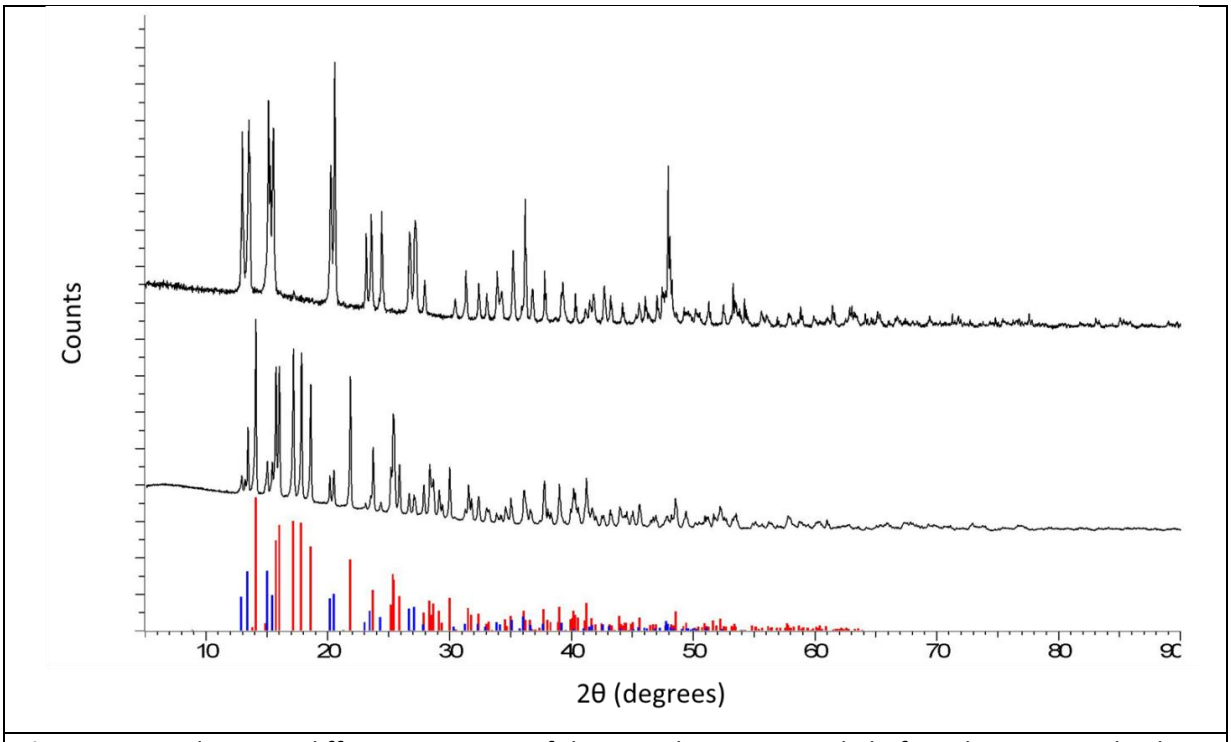

Figure 5. powder X-ray diffraction pattern of the uranyl nitrate sample before the time resolved IR measurements (top), and after the IR measurements (middle), calculated from the crystal structure of $UO_2(NO_3)_2(H_2O)_6$ (bottom, blue) and $UO_2(NO_3)_2(H_2O)_3$ (bottom, red).

Theoretical Calculations. DFT calculations were performed to study the structures of UNH and UNT, the transformation of UNH into UNT, and the IR properties of these species. Since limited experimental information is available on the H positions within these crystals, unit-cell models including all H-positions were built based on existing Crystallographic Information File (CIF) structures[12,13] and subsequently re-optimized using DFT (see Supplementary section for the corrected CIF files). Structures relaxed with DFT are shown in Figure 6 and their corresponding structural parameters are summarized in Table 1. As reported in Table 1, the computed equilibrium structures of UNH and UNT crystallize in the space groups $Cmc2_1$ (Z = 4) and $P\bar{1}$ (Z = 2), respectively, in good agreement with experiments; for the sake of completeness, the computed and experimental structural parameters of UND are also summarized in Table 1. The agreement between DFT methods and experiment is generally good; the relaxed unit-cell volume slightly overestimates the measured volumes by 1.3% for UNH and 4.7% for UNT, due to the fact that GGA calculations tend to overestimate the bond distances.

The known crystallographic constants and structural details for $UO_2(NO_3)_2(H_2O)_6$, $UO_2(NO_3)_2(H_2O)_3$ and the dihydrate $[UO_2(NO_3)_2(H_2O)_2]$ are all summarized in Table 1, along with crystallographic parameters calculated from DFT theory. It is worthy of note that in the orthorhombic group of the hexahydrate that the UO_2^{2+} cations all occupy equivalent positions,[12] whereas in the triclinic form of UNT, there are two distinct (inequivalent) unit cell positions for the uranyl moiety.[13] In this paper we try to assess the structure and stability of the hexahydrate vs. trihydrate phases, and correlate the changes to their infrared spectra using time-resolved reflectance spectroscopy. X-ray diffraction is used to confirm the starting and ending materials. The results are further corroborated using first-principles theoretical methods and optical microscopy to understand the UNH to UNT phase change properties.

Table 1. Measured and computed unit-cell parameters of Uranyl Nitrate structures. Distances are given in Å and angles in degrees.

Phase	**Space Group**	**XRD**		**DFT (This study)**	
$UO_2(NO_3)_2(H_2O)_6$	$Cmc2_1$	a = 13.197(3) [a] b = 8.035(2) [a] c = 11.467(3) [a]		a = 13.275 b = 8.044 c = 11.535	
$UO_2(NO_3)_2(H_2O)_3$	$P\bar{1}$	a = 7.0359(15) [b] b = 7.1730(15) [b] c = 10.084(2) [b]	α = 81.697(4) [b] β = 82.041(4) [b] γ = 63.642(4) [b]	a = 7.014 b = 7.440 c = 10.283	α = 82.45 β = 83.00 γ = 62.79
$UO_2(NO_3)_2(H_2O)_2$	$P2_1/c$	a = 14.124 [c] b = 8.432 [c] c = 7.028 [c]	β = 108 [c]	a = 14.180 b = 8.642 c = 7.129	β = 107.58

[a] Ref. 12; [b] Ref. 13; [c] Ref. 14.

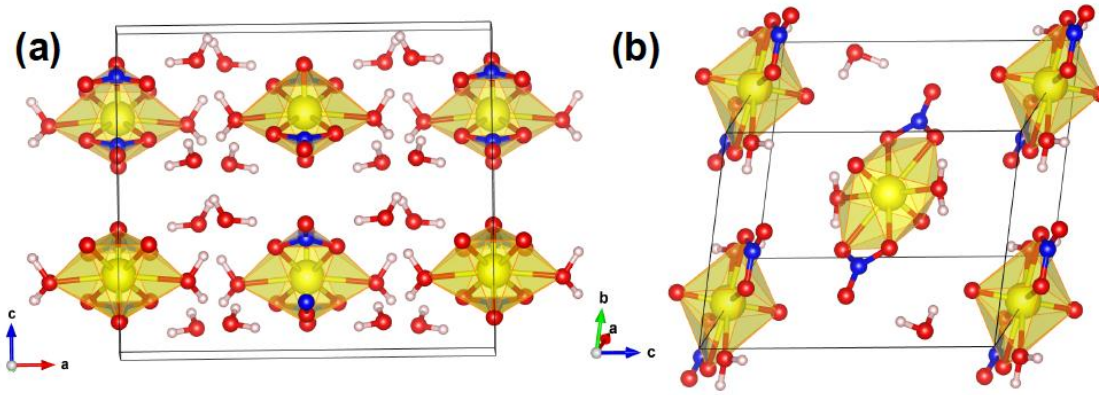

Figure 6. Ball-and-stick representation of the equilibrium structures of (a) $UO_2(NO_3)_2(H_2O)_6$ and (b) $UO_2(NO_3)_2(H_2O)_3$ relaxed at the GGA/PW91 level of theory. Color legend: O, red; U, yellow; N, blue; H, white. The U coordination polyhedra are shown in yellow and solid black lines indicate the unit cells.

The local environment of the U metal center (on 4*a* Wyckoff sites; *m*.. symmetry) in UNH is hexagonal bipyramidal with two short axial U=O bonds, calculated (measured) to be both at a distance of 1.806 Å (1.820 and 1.795 Å), and a nearly linear O=U=O angle of 179.0^o (177.58^o), and with equatorial oxygen atoms at distances of 2.466 Å (2.336 Å) for water oxygen atoms and 2.532 and 2.561 Å (2.651 Å) for oxygen atoms of the bidentate nitrate ligands. The predicted N–O···H–O–H contact distance between the nitrate groups and adjacent interstitial water molecules is 1.975 Å, while the H–O–H ···H–O–H contact distances between bound and interstitial water molecules are slightly shorter, i.e. 1.520 and 1.648 Å.

In UNT, the two uranyl sites are not equivalent: The hexagonal bipyramidal coordination environments of the U_1 are on 1*h* Wyckoff sites; $\bar{1}$ symmetry whereas the U_2 are on 1*d* Wyckoff sites with $\bar{1}$ symmetry centers. They consist of short pairs of axial bonds calculated (measured) to be U_1=O 1.811 Å (1.738 Å) and U_2=O 1.806 (1.745 Å), with O=U_1=O and O=U_2=O angles of 179.6 and 178.8^o (180^o for O=U_1=O and O=U_2=O), and with equatorial oxygen atoms at distances U_1–O: 2.475, 2.488 Å (2.453 Å) and U_2–O = 2.422, 2.506 Å (2.440 Å) for water oxygen atoms and U_1–O = 2.493, 2.497 Å (2.485 and 2.489 Å) and U_2–O = 2.472, 2.518 Å (2.473 and 2.539 Å) for oxygen atoms of the bidentate nitrate ligands. The calculated N–O···H–O–H contact distances between the nitrate groups and adjacent interstitial water molecules are in the range 2.722–3.216 Å, while the H–O–H ···H–O–H contact distances between bound and interstitial water molecules are *ca*. 2.49 Å.

Some of the small discrepancies noticed above between measured v. calculated bond distances and angles is ascribed in part to the overestimation of structural parameters in GGA calculations.

The complete infrared absorption spectra between 0 and 4000 cm^{-1} for UNH and UNT simulated from the vibrational frequencies and infrared intensities as calculated with DFPT are provided as supporting information in Figure S6. Regions of particular interest in this study are for the wavelength ranges 900–960 cm^{-1} and also 1200–1600 cm^{-1}; the latter depicted in Figure 7. A full-width at half-maximum (FWHM) parameter of 10 cm^{-1} was used for all simulation plots. The dominant computed vibrational modes in the 900–960 cm^{-1} domain are 918, 934 and 955 cm^{-1} for UNH and 920, 928 and 944 cm^{-1} for UNT. Normal mode analysis for UNH shows that the mode at 918 cm^{-1} corresponds to asymmetric stretch of O=U=O coupled with OH wagging in the equatorial water molecules whereas the mode at 934 cm^{-1} originates from the asymmetric stretching of O=U=O coupled with OH bending in the equatorial water molecules. The normal mode at 955 cm^{-1} is attributed to asymmetrical stretching of O=U=O coupled with the libration of water molecules.

For the UNT the mode at 920 cm^{-1} originates from the coupling of asymmetrical stretching of $O=U_1=O$ to the OH wagging of the equatorial water molecules whereas the mode at 928 cm^{-1} corresponds to the analogous mode (asymmetrical stretching of UO_2^{2+} cation coupled with OH wagging of equatorial waters) albeit from the uranyl group in the second position, i.e. the $O=U_2=O$ stretch. The mode at 944 cm^{-1} is due to the asymmetric stretch of the $O=U_1=O$ coupled with the libration of water molecules.

Table 2. Select Vibrational Mode Assignments in the Mid-Infrared for UNH and UNT

IR Absorbance Measured Deane et al.[30] (cm^{-1})	**IR Reflectance Measured** (cm^{-1})	**DFT Predicted Frequency** (cm^{-1})	**DFT Mode Description**
$UO_2(NO_3)_2(H_2O)_6$			
747 NO_3^- ν_3	748		
807 NO_3^- ν_6	808		
962/938 UO_2^{2+} ν_3	949	918	asym. O=U=O str coupled with OH wag in equatorial water molecules
		934	asym. O=U=O str coupled with OH bend in equatorial water molecules;

		955	asym. O=U=O str coupled with libration of water molecules.
1050/1041 NO_3^- ν_1	1039		
1339/1304 NO_3^- ν_4	1305	1278	NO_3 twist coupled w OH wagging in equatorial water molecules,
1339/1304 NO_3^- ν_4	1344	1310	NO_3 twist coupled w OH scissoring in equatorial water molecules
	1452		
	1463	1451	asym. O-N-O str. coupled with OH wag in equatorial water .molecules
1495 NO_3^- ν_2	1494	1473	
	1501	1493	Combo: asym. O-N-O str. plus water libration
	1511		
$UO_2(NO_3)_2(H_2O)_3$			
	744		
	799		
	957	920	asym. O=U_1=O str coupled with OH wag in equatorial water molecules
	966	928	asym. O=U_2=O str coupled with OH wag in equatorial water molecules;
		944	asym. O=U_1=O str coupled with libration of water molecules.
	1286	1225	NO_3 twisting bound to U_1
	1310	1274	NO_3 twisting bound to U_2
	1502	1482	NO_3 asym. str w/ H_2O libration
	1513	1513	NO_3 asym. str of NO_3 adjacent to U_2
	1549	1531	NO_3 asym. str adjacent to U_2 w/ bend of equatorial H_2O

While it is not strictly correct to compare intensities between infrared reflectance spectra vs. the DFT-predicted absorption spectra, calculated frequencies and relative intensity trends can be quite useful: While the predicted frequencies vary in general from the experimental values by ca. 3% in the 1200 – 1600 cm^{-1} domain, for the asymmetric uranyl stretch the trend suggested by the DFT theory matches fairly well what is seen in experiment: Upon dehydration of the hexahydrate to the trihydrate, the O=U=O asymmetric stretch splits due to the lower symmetry, with the two resultant bands shifting to frequencies +2 and +10 cm^{-1} higher as predicted by DFT; frequency

shifts of +8 and +17 cm^{-1} from the parent UNH reststrahlen band were measured in the experimental reflectance spectra (Figure 4).

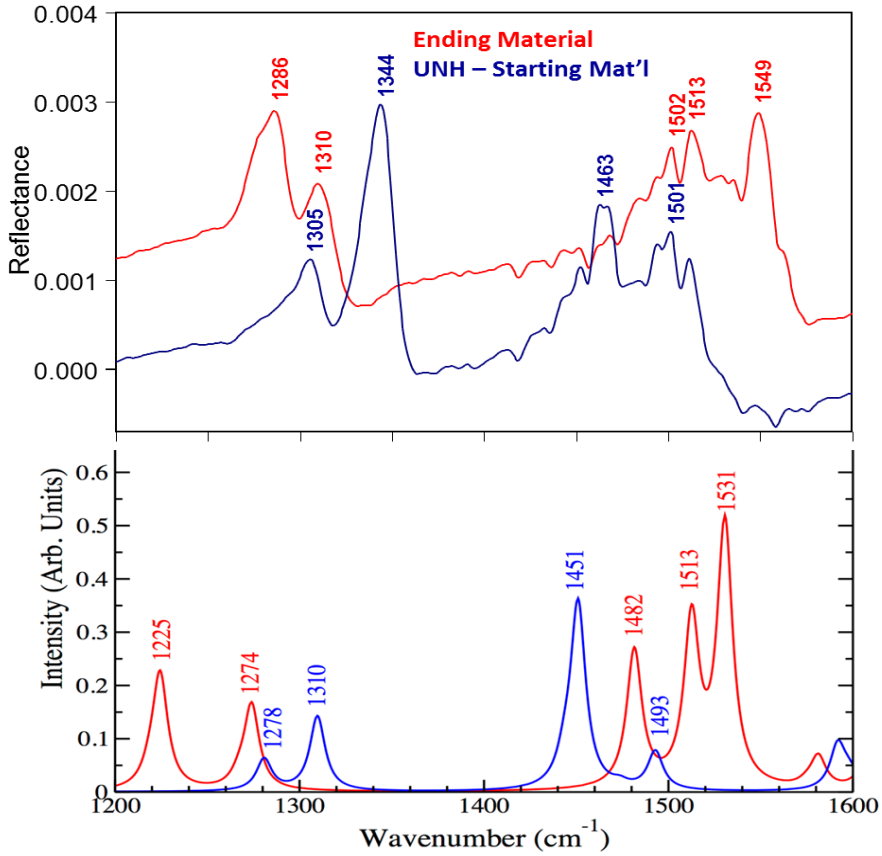

Figure 7. Top: Experimental directional-hemispherical reflectance spectra of the UNH starting material (blue trace) and UNT/UNH ending material in the 1200 to 1600 cm^{-1} region. Bottom: Simulated infrared absorption spectra of $UO_2(NO_3)_2(H_2O)_6$ (blue) and $UO_2(NO_3)_2(H_2O)_3$ (red) in the 1200 to 1600 cm^{-1} range calculated with DFPT at the GGA/PW91 level of theory.

In the spectral range from 1200 to 1600 cm^{-1} Figure 7 compares the DFT predicted infrared absorption bands (bottom) with the measured experimental reflectance (top). In both cases the hexahydrate starting material are the blue traces while the red traces are the trihydrate or the experimental end product, which was shown to be primarily trihydrate. We again note that any comparison of calculated absorption spectra to measured reflectance must proceed with caution; we are tacitly assuming that the experimental peaks are upward-going reststrahlen peaks, true for the uranyl asymmetric stretch, but only assumed for the other bands. Nevertheless, assuming upward-going peaks for the experimental data, it is seen that the absolute frequencies are in reasonably good agreement, and the observed frequency shifts upon dehydration from UNH to

UNT are in very good agreement for this part of the spectrum. Many of these bands have been previously assigned primarily as NO_3^- modes[9,30] as noted in Table 2. Bullock also investigated these by studying the spectra as both the ligand L and cation M were varied in complexes of the form $M_xUO_2L_y(NO_3)_2$. He noted[9] that as the symmetry falls from D_{3h} to C_{2v} as the NO_3^- free ion becomes a bidentate ligand to the metal, instead of just three all six modes of the nitrate ion become IR active. We assumed that the intensity and frequency shifts that arise depend on the adjacent waters in the cell, three of which are removed upon dehydration. We have previously seen significant peak shift or growth for OH-bending and torsional modes of given molecules depending very strongly on the degree of hydration, i.e. number of adjacent water molecules in the cell.[17,31,32]

The DFT predicted frequencies can be of utility for the mode assignments: In Figure 7, the predicted frequency for UNH for the mode at 1278 cm^{-1} stems from twisting of the nitrate ligands coupled with OH wagging in the equatorial water molecules; the frequency at 1310 cm^{-1} is due to twisting of the nitrate ligands coupled with OH scissoring in the equatorial water molecules; the mode at 1451 cm^{-1} originates from asymmetrical O-N-O stretching coupled with OH wagging in the equatorial water molecules and water libration; and the mode at 1493 cm^{-1} corresponds to a combination of asymmetrical O-N-O stretch and water libration.

For the case of UNT the calculations suggest a different set of assignments due to the inequivalency of the two uranyl groups and the changed local environment (Fig. 6). The normal mode predicted at 1225 cm^{-1} is attributed to twisting of nitrate ligands connected to U_1 whereas the mode at 1274 is due to twisting of the nitrate ligands connected to U_2. The mode at 1482 cm^{-1} corresponds to asymmetrical stretching of the nitrate ligands coupled with water libration; the mode at 1513 cm^{-1} corresponds to asymmetrical stretching of the nitrate ligands connected to U_2 coupled with OH bending in the equatorial water molecules. The mode at 1531 cm^{-1} results from asymmetrical stretching of the nitrate ligands connected to U_2 coupled with OH bending in the equatorial water molecules.

4. DISCUSSION

The $UO_2(NO_3)_2(H_2O)_6$ unit cell has just a single position for the uranyl group. There are four water molecules that are not bound to the uranyl group in UNH. In contrast, there are two symmetrically distinct and independent U^{VI} atoms in UNT both of which are part of linear

$(UO_2)^{2+}$ uranyl ions and coordinated by six equatorial O atoms. There is also one water molecule that is not bound to the uranyl group directly. [Similarly for UND there are also two different uranyl groups, but no unbound water molecules.] In our studies, the time-resolved reflectance IR reveal some of the nature of the change in the UNH to UNT transformation: Along with significant changes in other mid-IR features, particularly NO_3^- bands (Figs. 3 and 7), the UNH is characterized by changes to the reststrahlen band associated with the ν_3 band of the asymmetric uranyl stretch having a single reflectance feature at 949.0 cm^{-1}. As dehydration from UNH to UNT occurs, the reststrahlen feature shifts to higher frequencies and forms a doublet band with peaks at 957 and 966 cm^{-1}. The changes in the mid-infrared spectrum were complex but consistent with the removal of water molecules from the unit cell and reconfiguration of NO_3^- ligands. These important shifts have not been previously identified or resolved at such high spectral or temporal resolution, along with the relatively facile conversion of UNH to UNT. We also noted that for powders such as UNT the volume scattering dominates: the reflectance spectra tend to be strongly particle-size dependent with the smaller uranyl nitrate particle resulting in higher overall reflectivity. However, in terms of features that can be used for identifying the UNH to UNT transformation, the reststrahlen-type feature near 950 cm^{-1} and other mid-IR bands are clearly UNH/UNT specific, so we have demonstrated a faster and better method for identifying different uranyl nitrate phases.

The infrared spectra of UNH along with the related compounds UNT and UND have been reported many times.[7-11,28,38,39] However, almost all previous papers report transmission measurements only, and most of these show two absorption peaks for the asymmetric UO_2^{2+} stretch in the vicinity of 950 cm^{-1}. The two peaks are usually separated by ~30 cm^{-1} and both are ascribed to the ν_3 IR-active asymmetric stretch, distinct from the ν_1 symmetric uranyl stretch[11,38] near 875 cm^{-1}. Specifically, several early papers indicated that the UNH itself has a doublet band with peak frequencies at 965/942 cm^{-1} reported by Ohwada,[39] 964/933 by Hoekstra et al,[33] 962/938 cm^{-1} by Deane et al.[30] and in the first and most cited instance 964/937 cm^{-1} by Allpress and Hambly.[8] Most report similar frequencies for the tri- or di-hydrates, usually blue-shifted. A few authors list only a single value for the UNH uranyl asymmetric stretch including Gatehouse[7] et al. (939 cm^{-1}), Caldow[40] et al. (933 cm^{-1}), as well as McGlynn[10] et al. (941 cm^{-1}); again most list blue-shifted values for the lower hydrates. Our DFT calculations show the uranyl

asymmetric stretch mode coupled with OH wagging splitting from 918 cm^{-1} for UNH into 920 cm^{-1} (U_1) and 928 cm^{-1} (U_2) for UNT due to the two distinct UO_2^{++} positions, consistent with the experimental observations. The frequencies in the range 1100-1600 cm^{-1} are largely due to nitrate ligands that show peak splittings: the twisting mode at 1280 cm^{-1} for UNH becomes 1225 cm^{-1} (U_1) and 1274 cm^{-1} (U_2) for UNT, while the asymmetric stretch mode of NO in nitrate ligands at 1493 cm^{-1} for UNH splits into two modes at 1513 cm^{-1} (U_1) and 1531 cm^{-1} (U_2) for UNT. The DFT calculations thus partially explain the experimental observations of Figure 3b as to why certain new bands grow in such as the peaks at 1286 and 1549 cm^{-1} while other peaks disappear such as the bands at 1344 and 1462 cm^{-1} during the UNH-UNT transition.

We note that in most of these earlier works the data were recorded using dispersive instruments and many do not indicate the spectral resolution; the spectrometers of the day may not have had sufficient resolving power to distinguish species with peak separations of ≤ 8 cm^{-1} such as the 949 cm^{-1} (UNH), vs. 957/966 cm^{-1} (UNT), as well as the shoulder of the UNT peak, or peaks associated with other potential species such as the di-hydrate. It may be[20,25] that the spacing of the peaks in the absorbance spectra is greater than or less than the reflectance spectra splitting shown here, but comparable splittings can be expected. Based in part on better spectral resolution, but based also on reflectance mode measurements and the availability of X-ray diffraction patterns, we thus do not concur with the conclusion of the earlier infrared works[7] such as Allpress and Hambly[8] who noted minimal difference between the IR spectra of the hexahydrate and trihydrate, and concluded that UNH and UNT had similar structures. In the intervening years, the crystal structures[12-14] have clearly shown otherwise (cf. section 3.3), but also the infrared spectral resolution and sensitivity have greatly improved (Figure 3). It may also be ascribed to the fact that our spectra were recorded in time-resolved reflectance mode where it is easier to access the sample and assay its composition upon dehydration.

We again note that the IR transmission mode for solids usually requires pressing a KBr pellet or Nujol mull, and we suggest that it may not be possible to do this without (partially) desiccating the sample and/or metathesizing the counterions, e.g. Br^- for NO_3^-.[8,10,16] Indirect results from our attempts to prepare smaller UNH particles suggest that the mere grinding of a UNH sample for preparation as a KBr pellet or Nujol mull leads to desiccation or metathesis of the sample, depending on pressure and the laboratory humidity. That is to say, the UNH invariably forms

some UNT (or UND?) due to the lack of water in the process (e.g. KBr must be kept dry). Some of our preliminary experiments indicated that during the simple process of grinding the UNH turned it (partially) to the matte yellow powder of UNT and other species, depending on the RH in the laboratory. This was confirmed by XRD. We do note that Deane et al.[30] [Dean30] observed just one reflectance peak from a single crystal of UNH in ATR reflectance mode which showed strong polarization dependence, but they were also careful to point out that desiccation may be a potential cause of the peak shifting/splitting. With these observations borne in mind, we question the origin of the splitting of the uranyl ν_3 band which has variously been ascribed to Fermi splitting resonance,[9] correlation field effects,[39] or as Bullock pointed out,[11] unit cell coupling. In that paper Bullock did point out that the ν_3 vibration has only one allowed frequency as was seen for analogous compounds in solution, and that the solid-state splitting may be anomalous. We further point out that for most effects such as unit cell coupling that were ascribed as the source of the doublet peak, they should also manifest themselves for the ν_1 symmetric stretch in the Raman spectrum and this is not the case; the Raman spectrum[11,38] of UNH has only a single sharp band near 875 cm^{-1}.

Finally we note that in a similar study, Finch and Hawthorne[41] reported that the alteration of schoepite to 'dehydrate schoepite' proceeded by three steps. The initial loss of interlayer water resulting in the collapse of the structural layers, then atomic re-arrangement, followed by re-arrangement to a defect $(UO_2)(OH)_2$ sheet structure. The complete process liberated 12 moles of H_2O for every mole of schoepite consumed. Any stress was observed to induce the dehydration, including heat, sunlight, and mechanical pressure. It was suggested that the lattice strain resulting from the initial dehydration induced further transformation of the starting material. Similar observations have been made with UNH, where dehydration can be accelerated by crushing and grinding the material.

5. SUMMARY

In this paper we have made seminal reflectance infrared observations of uranyl nitrate during the desiccation of the hexahydrate to the trihydrate, possibly even to the dihydrate. Time-resolved infrared reflectance spectroscopy was employed, and proved a superior approach to such dehydration studies. We report direct observation of phase transformation from

$UO_2(NO_3)_2(H_2O)_6$ to $UO_2(NO_3)_3(H_2O)_3$ through high resolution reflectance IR measurements and *in situ* optical microscopy imaging, with absolute confirmation of the phase mixture via XRD. The study confirms previous investigations that with decreasing relative humidity, the $UO_2(NO_3)_2(H_2O)_6$ will recrystallize as UNT accompanied by a structural change. The infrared reflectance spectrum can be used as a telltale of the phase state with the hexahydrate having a single reststrahlen reflectance band at 949 cm^{-1}, the trihydrate a weaker doublet at 966/957 cm^{-1}. There are very significant shifts throughout the 1200 to 1600 cm^{-1} region as well and the overall reflectivity increases with the formation of the matte powder. DFT calculations confirm the peak splitting of the uranyl asymmetric stretch mode in UNT that can serve as a signature of UNT during the UNH-UNT transition. The frequencies in the range 1200-1600 cm^{-1} (largely due to nitrate ligands) show significant normal mode changes which help explain the growth of the peaks at 1286 and 1549 cm^{-1} and the disappearance of the peaks at 1344 and 1462 cm^{-1} during the UNH-UNT transition. Further study of the UNH/UNT phase transition, particularly of the shifts for the infrared and Raman frequencies, is clearly warranted.

ASSOCIATED CONTENT

*Supporting Information

Infrared spectroscopy, *in-situ* movie of transformation with optical microscopy. This material is available free of charge via the Internet at >???.

AUTHOR INFORMATION

Corresponding Author

*E-mail: Timothy.Johnson@pnnl.gov Tel.: 509 372 6058.

Notes: The authors declare no competing financial interest.

ACKNOWLEDGEMENTS

The research described in this paper was supported in part by the U. S. Department of Energy Office of Nonproliferation and Verification Research and Development (NA-22). PNNL is operated by Battelle for the U.S. DOE under Contract DE-AC05-76RLO1830. We gratefully thank our sponsors for their support. Sandia National Laboratories is a multiprogram laboratory operated by Sandia Corporation, a wholly owned subsidiary of Lockheed Martin Company, for

the United States Department of Energy's National Nuclear Security Administration under Contract DE-AC04-94AL85000.

6. References

[1] Bordere, S.; Rouquerol, F.; Llewellyn, P. L.; Rouquerol, J., *Thermochim. Acta.* **1996**, *282/283*, 1-11.

[2] Kalekar, B. B.; Rajagopalan, K. V.; Pillai, C. G. S.; Ravindran, P. V., *J. Nucl. Mater*. **2000**, *279*, 245-252.

[3] Lodding, W.; Ojamaa, L., *J. Inorg. Nucl. Chem.*, **1965**, *27*, 1261-1268.

[4] Moseley, P. T.; Seabrook, C. J., *J. Chem. Soc., Dalton Trans.* **1973**, *10*, 1115-1120.

[5] Smith, W. H., *J. Inorg. Nucl. Chem*. **1968**, ***30***, 1761-1768.

[6] Smith, M. L.; Topley, B., *Proc. R. Soc. Lond. A.* **1931**, *134*, 224-245.

[7] Gatehouse, B. M.; Comyns, A. E., J. Chem. Soc. **1958**, part IV, *1958,* 3965-3971.

[8] Allpress, J. G.; Hambly, A. N., *Aust. J. Chem.* **1959**, *12*, 569-574.

[9] Bullock, J.I., J. Inorg. Nucl. Chem. **1967**, 29, 2257-2264.

[10] McGlynn, S.P., Smith, J.K., Neely, W.C., J. Chem. Phys. **1961,** 35, 105.

[11] Bullock, J.I., *J. Chem. Soc. (A)*, **1969,** 781.

[12] Taylor J. C.; M. H. Mueller, *Acta Cryst.* **1965**, *19*, 536-543.

[13] Hughes K-A.; P. C. Burns, *Acta Cryst*. **2003**, *C59*, i7-i8.

[14] Dalley, N. K.; Mueller, M. H.; Simonsen, S. H., *Inorg. Chem.* **1971**, *10*, 323-328.

[15] Burns, P. C.; Miller, M. L.; Ewing, R. C., *Can. Mineral.* **1996**, *34*, 845-880.

[16] Johnson, T.J.; Hipps, K.W.; Willett, R.D., *J. Phys. Chem*. **1988**, *92*, 6892-6899.

[17] Sweet, L. E.; Blake, T. A.; Henager, Jr., C. H.; Hu, S.; Johnson, T. J.; Meier, D.E.; Peper, S. H.; Schwantes, J. M., *J. Radioanal. Nucl. Chem.* **2012**, *296*, 105-110.

[18] Blake, T.A., Johnson, T.J., Tonkyn, R.G., Forland, B.M., Myers, T.L., Brauer, C.S., Su, Y.-F., *Proc. SPIE* 2014, *9073*, 907303-1.

[19] Myers, T.L.; Brauer, C. S.; Su, Y.-F.; Blake, T. A.; Johnson, T. J.; Richardson, R.L., in Algorithms and Technologies for Multispectral, Hyperspectral, and Ultraspectral Imagery XX, M. Velez-Reyes, F.A. Kruse, editors, Proc. SPIE, **2014**, *9088*, 908809-1.

[20] T.L. Myers, C.S. Brauer, Y.-F. Su, T. A. Blake, R.G. Tonkyn, A.B. Ertel, T.J. Johnson and R.L. Richardson, "Quantitative Reflectance Spectra of Solid Powders as a Function of Particle Size," *Applied Optics*, **2015**, *54*, 4863-4875.

[21] Perdew, J. P.; Wang, Y., *Phys. Rev. B.* **1992**, *45*, 13244-13249.

[22] Weck, P. F.; Kim, E.; Masci, B.; Thurery, P.; Czerwinski, K. R., *Inorg. Chem*. **2010**, *49*, 1465-1470.

[23] Weck, P. F.; Kim, E.; Jove-Colon, C. F.; Sassani, D. C. *Dalton Trans*. **2012**, *41*, 9748-9752.

[24] J. E. Bertie, J.E., Zhang S.L. Keefe, C.D. *Vibrational Spectroscopy*, **1995,** 8, 215-229.

[25] Moersch, J. E.; Christensen, P. R., *J. Geophys. Res.* **1995**, *100(E4)*, 7465-7477.

[26] Y.-F. Su, T.L. Myers, C.S. Brauer, T.A. Blake, B.M. Forland, J.E. Szecsody, T.J. Johnson, "Infrared reflectance spectra: Effects of particle size, provenance and preparation," Proc. SPIE, **2014**, 9253, 9253-3

[27] Salisbury, J. W.; Walter, L. S., *J. Geophys. Res.* **1989**, *94*, 9192-9202.

[28] Salisbury, J. W., Wald, A., *Icarus* **1992**, *96*, 121-128.

[29] Cooper, B. L.; Salisbury, J. W.; Killen, R. M.; Potter, A. E., *J. Geophys. Res.* **2002**, *107(E4)*, 1-17.

[30] Deane, A.M., Richards, E.W.T., Stephen, I.G., *Spectrochim. Acta,* **1966,** 22, 1253-1260.

[31] Johnson, T.J.; Williams, S.D.; Valentine, N.B.; Su, Y.-F., *Applied Spectroscopy* **2009**, *63(8)*, 908-815.

[32] Johnson, T.J.; Williams, S.D.; Valentine, N.B.; Su, Y.-F., *Vib. Spectr.* **2010**, *53*, 28–33.

[33] Hoekstra, H. R.; Siegel, S., *J. Inorg. Nucl. Chem.* **1961**, *18*, 154-165.

[34] Hoekstra, H. R., *Inorg. Chem.* **1963**, *2*, 492-495.

[35] Mustard, J. F.; Hays, J. E., *Icarus* **1997**, *125*, 145-163.

[36] Bras, A. L.; Erard, S., *Planetary and Space Sci.* **2003**, *51*, 281-294.

[37] Hapke, B., *J. Geophys. Res.* **1996**, *101(E7)*, 16833-16840.

[38] Palacios, M.L., Taylor, S.H., *Applied Spectroscopy,* **2000**, *54(9),* 1372-1378

[39] Ohwada, K., Spectrochimica Acta, **1979,** 35A, 1283-1288

[40] Caldow, G.L., van Cleve, A.B., Eager, R.L., *Can J. Chem.* **1960,** 38, 772-782.

[41] Finch, R. J.; Hawthorne, F. C. *Can. Mineral.* **1998**, *36*, 831-845

Supplementary Information

Specimens of uranyl nitrate hexahydrate recovered by recrystallization was collected and ground. A subset of this sample was collected and then re-dissolved in 1 mL of 18 MΩ·cm DI H_2O and allowed to come to an equilibrated mass of 0.66088 g at 23.9 °C and 31% RH in a (20.26 cm^2) glass dish placed atop a Mettler-Toledo scale, while exposed to laboratory atmosphere. It took several days of exposure under these conditions for the mass to stabilize. After the mass no longer changed, 600 µL of 18 MΩ·cm DI H_2O was added to the cake-like uranyl nitrate which resulted in a mass of 1.21432 g defined as time t=0. Following the addition of water, the sample remained on the scale and the mass was monitored intermittently over an extended period of time and plotted (Fig. 1).

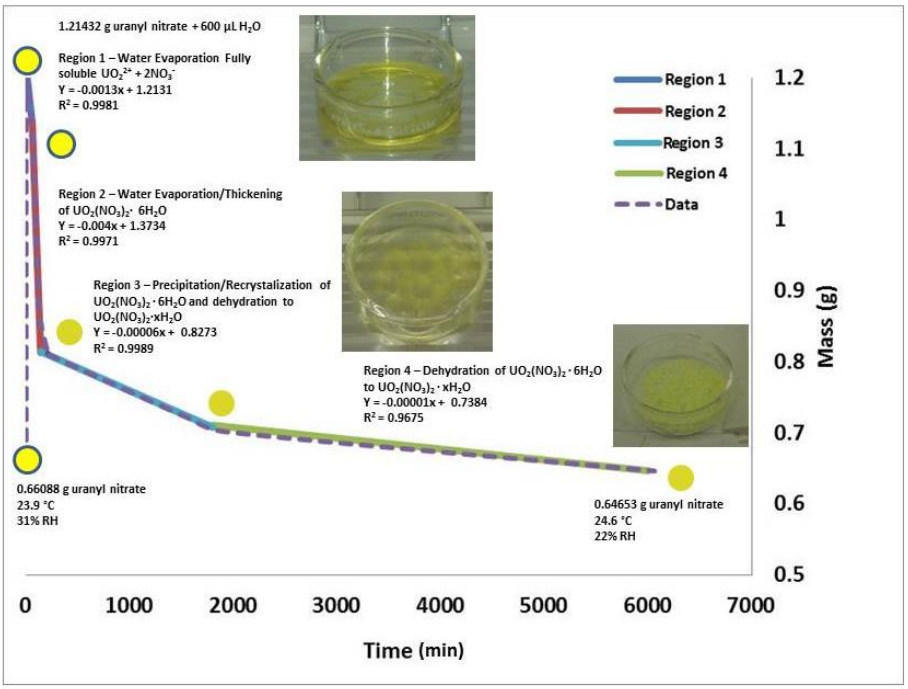

Figure S1. Mass loss of UNH/UNT

Four regions of dehydration were observed (Fig. 1) and their relative mass loss rates are reported in Table 3. Region 1 vaporizes water at a predictable rate where Region 2 dehydrates water at a rate of approximately 3× that of Region 1. In Region 3 appreciable quantities of uranyl nitrate began to recrystallize, where upon swirling would rapidly dissolve in the excess free water – this process ends as Region 4 is approached and the kinetic rate of mass loss slows by a factor of 66×. Eventually, Region 4 began to manifest in which the wet uranyl nitrate that recrystallized

in Region 3 begins to dry into a yellow cake at a rate of 6× slower than region 3 alone. The pure evaporation of water happens predictably while the conversion of final mass of the sample is dependent upon relative humidity, though the rate of evaporation is dependent upon the temperature of the environment and exposed surface area of the sample being dehydrated.

Table S1. Kinetic mass rates per time domains for 31% RH at 23.9°C.

Region	Mass loss rate (mg H_2O/min)	Rate ratio
1	-1.30	N/A
2	-4.00	3.1
3	-0.06	66.7
4	-0.01	6.0

Optical microscopy was performed to show the recrystallization of the UNT from UNH. The loss of water from the structure results in complete irreversible transformation.

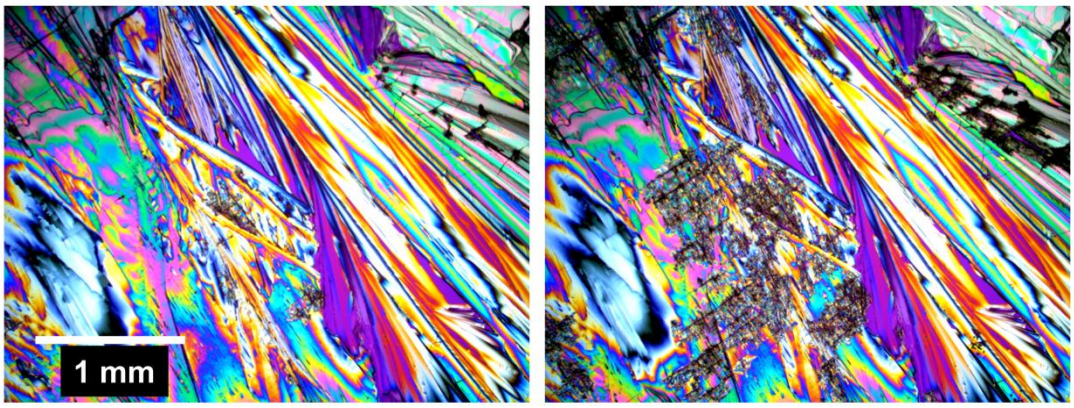

Figure S3. Rapid transformation of hexahydrate to trihydrate observed in the optical microscope

Monitoring of the much slower dehydration of UNT, suggests a potentially reversible process. The overall structure does not change significantly during this process. The images show reversal of polarization in the crystals during dehydration.

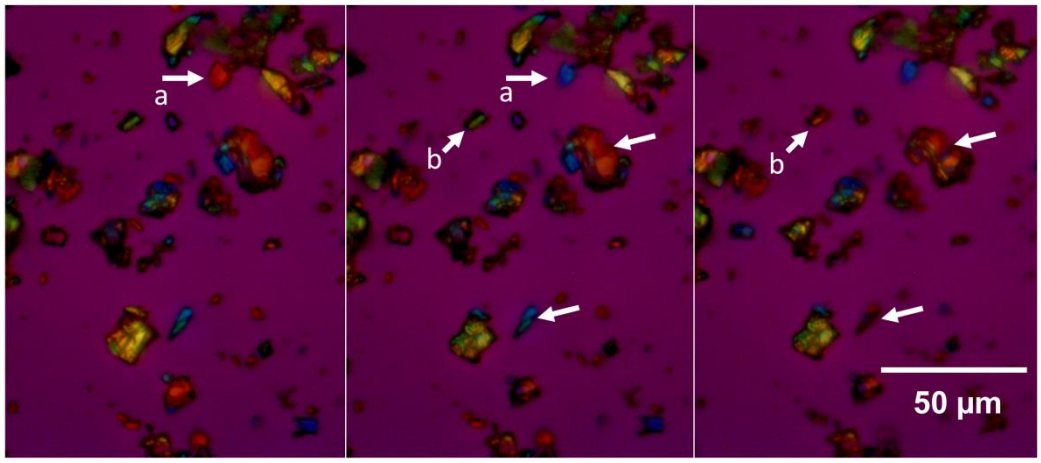

Figure S4. Optical micrograph of a partial phase transformation of trihydrate to dihydrate

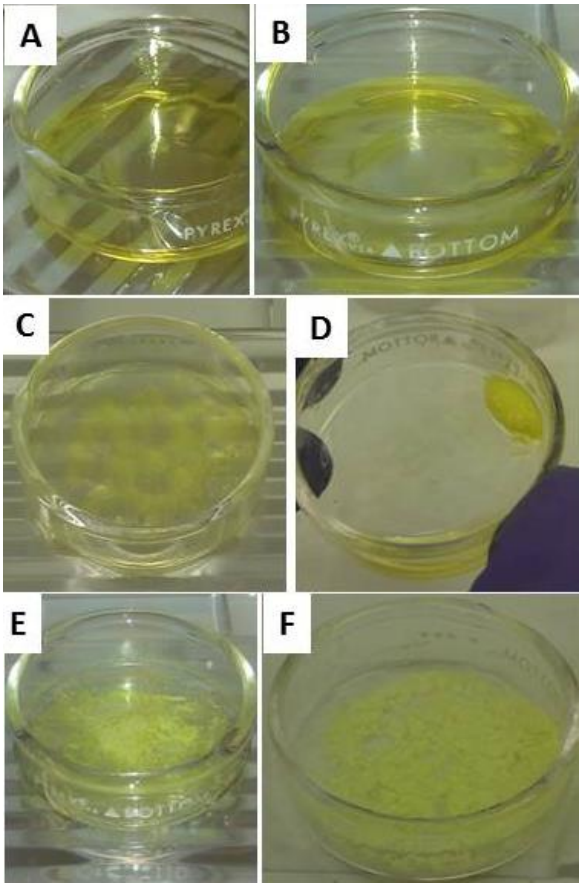

Figure S5. Images of soluble uranyl nitrate (A/B) followed by recrystallization (C/D) then dehydration (E/F) at 21-22°C, 44%RH over 72 hours.

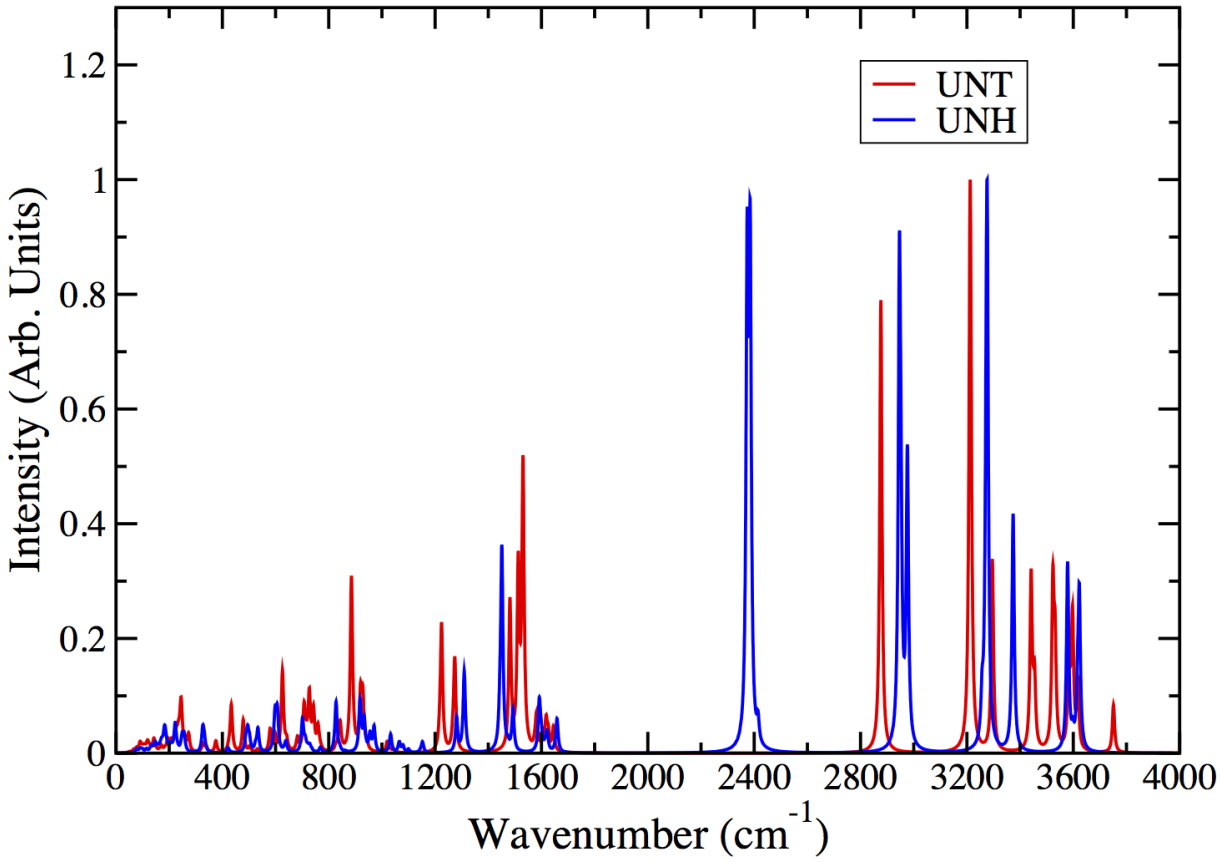

Figure S6. Simulated vibrational spectra of $UO_2(NO_3)_2(H_2O)_6$ (blue) and $UO_2(NO_3)_2(H_2O)_3$ (red) in the range 0–4000 cm^{-1} calculated with DFPT at the GGA/PW91 level of theory.